Journal of Organometallic Chemistry 932 (2021) 121644

Contents lists available at ScienceDirect

Journal of Organometallic Chemistry

journal homepage: www.elsevier.com/locate/jorganchem

An aggregation-induced phosphorescent emission-active iridium(III) complex for fluoride anion imaging in living cells

Zejing Chen[a,b,‡], Jiayang Jiang[b,‡], Weili Zhao[b], Xiaoming Hu[a], Mingjuan Xie[b], Feiyang Li[b], Shujuan Liu[b,**], Qiang Zhao[b,*]

[a] Jiangxi Key Laboratory for Nanobiomaterials, Institute of Advanced Materials (IAM), East China Jiaotong University (ECJTU), 808 Shuanggang East Main Street, Nanchang 330013, P. R. China

[b] Key Laboratory for Organic Electronics and Information Displays & Jiangsu Key Laboratory for Biosensors, Institute of Advanced Materials (IAM), Nanjing University of Posts and Telecommunications (NJUPT), 9 Wenyuan Road, Nanjing 210023, P. R. China

ARTICLE INFO

Article history:
Received 12 September 2020
Revised 25 October 2020
Accepted 1 December 2020
Available online 2 December 2020

Keywords:
Iridium(III) complex
Aggregation-induced phosphorescent emission
Fluoride anion
Probe
Time-resolved photoluminescence imaging

ABSTRACT

Fluoride anion plays a crucial role in bone and tooth growth. However, overdose of fluoride anion can also lead to many chronic diseases and there is no specific medicine for fluorosis so far. Hence, the early detection and accurate estimation of fluoride anion intake are important. In this work, an aggregation-induced phosphorescent emission (AIPE)-active iridium(III) complex as fluoride anion probe (**Ir-AF**) has been developed by incorporating *N*-(4-hydroxylphenyl)-rhodol protected by tert-butyldiphenylsilyl onto cyclometalating ligand. As **Ir-AF** reacts with fluoride anion, the nonradiative transitions of **Ir-AF** would be promoted by enhanced photoinduced electron transfer effect and intramolecular rotations, leading to its phosphorescence quenching dramatically. Thus, **Ir-AF** has been used for fluoride anion measurement in the aqueous solution by ratiometric readout. Furthermore, with the utilization of the long-lived phosphorescence from **Ir-AF**, fluoride anion sensing in living cells with high signal-to-noise ratio has been achieved by time-resolved photoluminescence imaging. This is the first report of AIPE-active probe for fluoride anion.

1. Introduction

Fluorine is an essential trace element for human body. Owing to its strong electronegativity, fluorine is almost in valence state of negative one in the nature, such as fluoride anion (F^-), which is considered as the largest source to daily fluorine intake [1]. Fluoride anion can promote bone growth and is closely related to the osteoporosis and odontopathy [2,3]. In the past, the addition of fluoride anion to water to ensure fluorine intake is a common practice [4,5]. And it is also added to toothpastes to reduce the dental cavities and strengthen the resistance of teeth to acid corrosion [6,7]. However, studies have shown that overintake of fluoride anion can lead to not only mottled enamel and skeletal fluorosis but acute gastric, nephrotoxic changes, brain and immune system damage [8-11]. As there is no specific medicine for fluorosis so far, the early detection and accurate estimation of fluoride anion are of great significance.

To date, atomic absorption spectrometery, ion chromatography, ^{19}F nuclear magnetic resonance, inductively coupled plasma mass spectrometery, reverse phase high performance liquid chromatography, molecular absorption spectrometery are available approaches to detect fluoride anion [12-15]. In addition, luminescence detection and imaging have attracted more and more attention because of their good selectivity, high sensitivity, superb spatial resolution and relatively low cost [16-20]. By a non-invasive way, luminescence detection and imaging could be used to detect the target analytes in micromole or even nanomolar levels in intact living samples in real time, which is in favor of biological processes study. Consequently, they usually require appropriate probes.

As candidates for luminescent probes, phosphorescent transition-metal complexes (PTMCs), especially iridium(III) system have many advantages, such as high luminescence quantum yields, excellent photostability, tunable emission, various sensitive charge-transfer states [21,22]. Moreover, they possess long-lived phosphorescence which could be easily screened out from complicated environments with short-lived background fluorescence or autofluorescence from biological samples via time-resolved

* Corresponding author.
** Corresponding author.
E-mail addresses: iamsjliu@njupt.edu.cn (S. Liu), iamqzhao@njupt.edu.cn (Q. Zhao).
‡ Chen and Jiang contributed equally to this work

https://doi.org/10.1016/j.jorganchem.2020.121644
0022-328X/

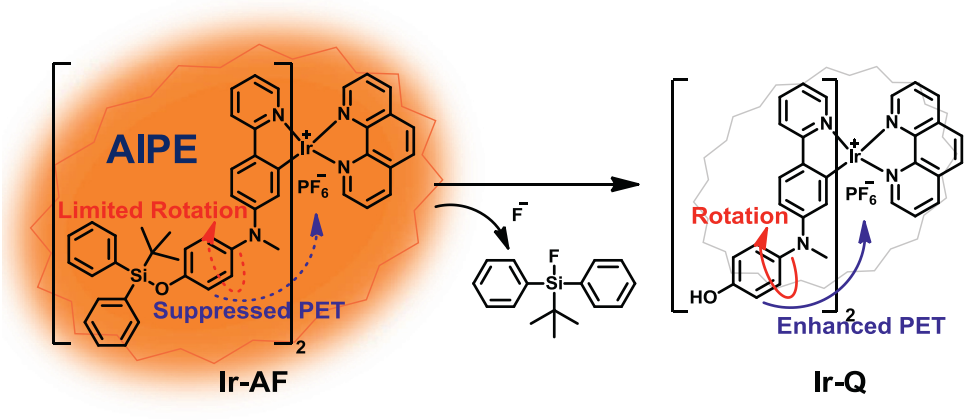

Fig. 1. Chemical structure of **Ir-AF** and schematic illustration for detecting fluoride anion.

photoluminescence imaging (TRPI) technique, like photoluminescence lifetime imaging microscopy (PLIM) and time-gated photoluminescence imaging (TGPI), thus achieving reliable optical detection [23]. In the past years, lots of luminescent probes based on PTMCs have been reported [24-27]. Our research group have also developed a series of iridium(III) complex bioprobes, including fluoride anion probes [28-31]. However, the propensity of PTMCs to aggregate in poor solvent sometimes may cause severe triplet-triplet annihilation (TTA) which often occurs in the solid state, leading to aggregation-caused quenching (ACQ). On the contrary, aggregation-induced emission (AIE) that is an unusual photophysical phenomenon of luminescent materials could break the limitations that the materials are not suitable for luminescent application in the solid state or at a high concentration [32,33]. In 2008, our group first conducted an in-depth research about the aggregation-induced phosphorescent emission (AIPE) mechanism based on two octahedral cyclometalated Ir(III) complexes [34]. Then, there has been a rising interest in developing AIPE-active PTMCs and exploring their applications [35-43].

In our recent study, *N*-(4-hydroxylphenyl)-rhodol moiety grafted onto the cyclometalating ligand have been found to facilitate the nonradiative transitions of phosphorescent iridium(III) complexes by the photoinduced electron transfer (PET) effect and intramolecular rotations [44]. We speculated that introducing moieties which could restrain PET effect imposed by the electron-rich hydroxyphenyl group or alleviate intramolecular rotations may recover the efficient phosphorescence of the related iridium(III) complexes. In this work, an cationic iridium(III) complexes (**Ir-AF**) containing tert-butyldiphenylsilyl (TBDPS) moieties on the oxygen atom of the *N*-(4-hydroxylphenyl)-rhodol has been designed and synthesized (Fig. 1). As **Ir-AF** possesses the characteristics of AIPE, it has been used for fluoride anion measurement in the aqueous solution by ratiometric readout. Importantly, utilizing the long-lived phosphoresncence of **Ir-AF**, accurate fluoride anion sensing in living cells was achieved by time-resolved photoluminescence imaging. To the best of our knowledge, this is the first report of AIPE-active probe for fluoride anion.

2. Experimental section

All the raw materials and reagents were purchased from commercial suppliers and used without further purification except some were noted. All solvents were purified and dried under reflux over CaH_2 and used freshly. All aqueous solutions were prepared with deionized water. The structure of **Ir-AF** was characterized by ^{1}H NMR and autoflex matrix-assisted laser desorption ionization time-of-flight (MALDI-TOF) mass spectrometry. The UV-visible absorption spectra and emission spectra were conducted with a Shimadzu UV-3600 spectrophotometer and Edinburgh FL 920 spectrophotometer, respectively. Besides, an integrating sphere was employed to collect data of absolute quantum yields in N_2 atmosphere. Luminescence lifetime of compounds were measured through a semiconductor laser unit on Olympus Edinburgh LFS-920 spectrometer. Time-resolved photoluminescence imaging experiments were conducted on an Olympus FV1000 laser scanning confocal microscope and the lifetime data was processed by correlative and professional software provided by Becker & Hickl GmbH Company. Moreover, cell flow cytometer analysis was carried out with FlowSight imaging flow cytometer. The details of experimental section were shown in the supplementary data.

3. Results and discussion

3.1. Synthesis and characterization

The chemical structure of iridium(III) complex **Ir-AF** is shown in Scheme 1, which was confirmed by NMR and mass spectra. Briefly, the skeleton of cyclometalating HC^*N* ligand (4-((tert-butyldiphenylsilyl)oxy)-N-(4-(pyridin-2-yl)phenyl)aniline) was prepared in high yield via a Buchwald–Hartwig coupling reaction of aryl trifluoromethanesulfonate with aniline derivatives [45]. Then, **Ir-AF** was synthesized according to the typical three-step method for cationic iridium(III) complex [46]: the cyclometalated iridium(III)-chlorobridged dimers $(C^N)_2Ir(\mu\text{-}Cl)_2Ir(C^N)_2$ were prepared by refluxing iridium trichloride with cyclometalating HC^*N* ligand, which was treated with 1,10-phenanthroline (*N^N* ligand) without further purification, followed by counterion exchange reaction from chloride ion to hexafluorophosphate anion. The detailed synthetic routes and characterization data for complex **Ir-AF** and corresponding intermediates are presented in the supplementary data.

3.2. Photophysical properties

The photophysical properties of **Ir-AF** have been studied by UV-vis absorption and photoluminescence spectra in different solvents, and the photophysical data are summarized in Table S1 and S2. As depicted in Fig. 2a, the strong absorption bands below about 310 nm are assigned to $^1\pi\text{–}\pi^*$ transitions of the cyclometalating ligands. The moderately intense absorption bands over about 310–450 nm are attributed to the spin-allowed singlet metal-to-ligand charge-transfer (^{1}MLCT) and ligand-to-ligand charge-transfer (^{1}LLCT) transitions. The extremely weak absorption bands above about 450 nm are originated from the mixed ^{1}MLCT

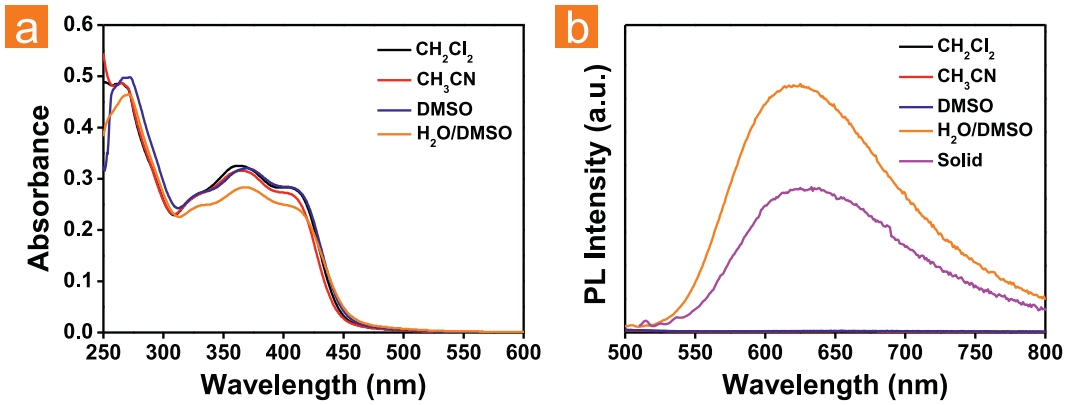

Fig. 2. Absorption spectra (a) and emission spectra (b) of **Ir-AF** in dichloromethane, acetonitrile, dimethylsulfoxide, water (contain 10% dimethylsulfoxide) or solid state, respectively.

and spin-forbidden triplet metal-to-ligand charge-transfer (^{3}MLCT) transitions [47]. It is worth noting that the absorption spectra profiles of **Ir-AF** in three kinds of good solvents (dichloromethane, acetonitrile and dimethylsulfoxide) are similar, while the absorption in aqueous solution shows a little weaker, which may be arised from the slight aggregation of **Ir-AF** in poor solvent. The photoluminescence spectra at ambient temperature were recorded in the air (Fig. 2b). Upon photoexcitation at 405 nm, the emission of **Ir-AF** could hardly be observed in three good solvents. In contrast, **Ir-AF** displayed an intense band with the peak around 622 nm (Φ = 0.045) in aqueous solution (contain 10% dimethylsulfoxide). This featureless and broad band, which could be assigned to ^{3}MLCT transitions, is similar to the emission band of **Ir-AF** in the solid state (Φ = 0.012), indicating that the phosphorescence of **Ir-AF** is probably induced by aggregation.

3.3. Aggregation-induced phosphorescent emission

The AIPE characteristics of **Ir-AF** have been investigated by emission spectra in a dimethylsulfoxide/water mixed solvent system with different water fractions at room temperature. As shown in the Fig. 3a, no emission band of **Ir-AF** was observed in dimethylsulfoxide solution, and the emission intensity nearly kept constant even when the water fraction was less than 40%. Nevertheless, the phosphorescence intensity at around 622 nm was dramatically enhanced to maximum when the water fraction increases from 40% to 50% (Fig. 3b). Dynamic light scanning (DLS) and Transmission electron microscopy (TEM) analyses revealed an average diameter of 72 nm for **Ir-AF** dispersed in above mixed solution (Fig. 3c). These results implied that the emission of **Ir-AF** is indeed induced along with aggregate formation. Notably, at the water fraction of above 50%, the phosphorescence intensity gradually decreases as water content rose. This phenomenon may be explained by TTA, which was further proved by significantly increased effective diameter and polydispersity index measurements in solution with increasing water content (Fig. S1).

To further confirm the AIPE behavior of **Ir-AF** and explore whether the potential hypoxic effect formed in aggregation is the other factor for promoting emission of **Ir-AF**, the emission spectra in three good solvents in the absence and presence of O_2 were investigated. As described in the Fig. 3d, the emission band of **Ir-AF** in six conditions could be hardly detectable, which indicated the emission of **Ir-AF** cannot be activated in good solvents even though in the hypoxic environment. In general, the phosphorescence from iridium(III) complexes could be quenched by oxygen molecule and are susceptible to oxygen content in the environment, as depicted in Fig. 3e. Thus, the results mean that the emission of **Ir-AF** is dominantly AIPE-active in aqueous solution, and the hypoxic effect accompanying with aggregate formation could be ignored in the air. Additionally, the photobleaching experiments in which the solution is under the illumination of 405 nm laser source have been carried out (Fig. 3f). Compared with the gradually decreasing intensities of commercial dyes (Hoechst and Lyso-Tracker Red), the phosphorescence intensity at 622 nm did not show obvious decrease within 20 min, suggesting that **Ir-AF** has a good photostability and its AIPE properties are steady.

3.4. Mechanism of fluoride anion detection

Considering that tert-butyldiphenylsilyl (TBDPS) moieties on the oxygen atom of the phenol are often used as the candidate recognition sites for fluoride anion, the response of **Ir-AF** toward fluoride anion was evaluated preliminarily. The product extracted from the reaction mixtures of iridium(III) complex and fluoride anion has been studied by matrix-assisted laser desorption ionization time-of-flight mass spectrometry. As shown in Fig. 4, the molecular weight of products is 478 less than that of **Ir-AF**, which were consistent with the expectation that the desilylation process occurred in the reaction. The main products possessing phenol moieties generated in the above reactions were also verified by ^{1}H NMR spectra (Fig. S2). Therefore, the significantly reduced phosphorescence can be attributed to PET process, which is consistent with the previous reports [28,29].

3.5. Fluoride anion sensing properties

The phosphorescence intensity and lifetime response of **Ir-AF** to fluoride anion in dimethylsulfoxide/water (V/V = 1/9) mixed solution has been studied in detail by spectrofluorometric titrations. As shown in Fig. 5a, a gradual dose dependent phosphorescence diminishment was observed with the sequential addition of fluoride anion. When fluoride anion concentration reached 5 μM, the phosphorescence intensity at 622 nm dropped to half compared with those in the absence of fluoride anion. Meanwhile, the phosphorescence lifetime decreased from 213 ns to 168 ns (Fig. 5b). Upon addition of 20 μM fluoride anion, the emission bands nearly disappeared and the quenching efficiencies (defined by the equation $\eta = (I_0\text{-}I)/I_0$, I_0 and I denote the phosphorescence intensity before and after the addition of fluoride anion, respectively.) reached 97%. The phosphorescence lifetime shortened to 113 ns accordingly. Concomitantly, the phosphorescence intensity ratio (I/I_0) varied with an approximate linear relationship in fluoride anion concentration range of 0–8 μM (Fig. 5c). The related detection limitation is calculated to be (2.6×10^{-2} μM), suggesting the sensitivity

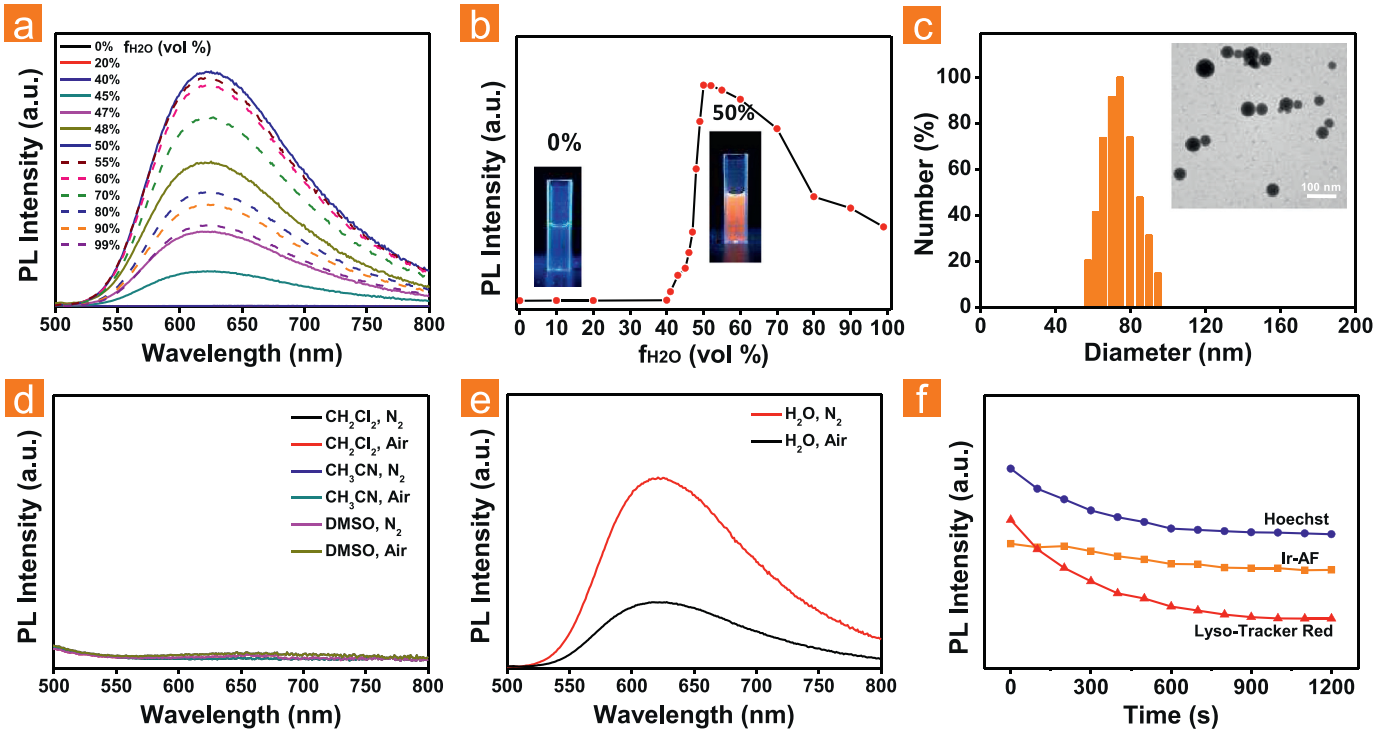

Fig. 3. (a) Emission spectra of **Ir-AF** (10 μM) in dimethylsulfoxide solution added with different fraction of water (λ_{ex} = 405 nm). (b) Plot of $I_{622\ nm}$ as a function of H_2O fraction. The insert pictures were **Ir-AF** in dimethylsulfoxide solution (left) and in dimethylsulfoxide /water (v/v=1:1) solution (right). (c) DLS analysis of **Ir-AF** in aqueous solution. (d) Emission spectra of **Ir-AF** (10 μM) in dichloromethane, acetonitrile and dimethylsulfoxide saturated with air or N_2, respectively. (e) Emission spectra of **Ir-AF** (10 μM) in aqueous solution saturated with air or N_2, respectively. (f) Continuously monitoring luminescence intensities of **Ir-AF** at 622 nm, Hoechst at 460 nm and Lyso-Tracker Red at 590 nm in aqueous solution within 20 min, respectively. Excitation wavelength was 405 nm.

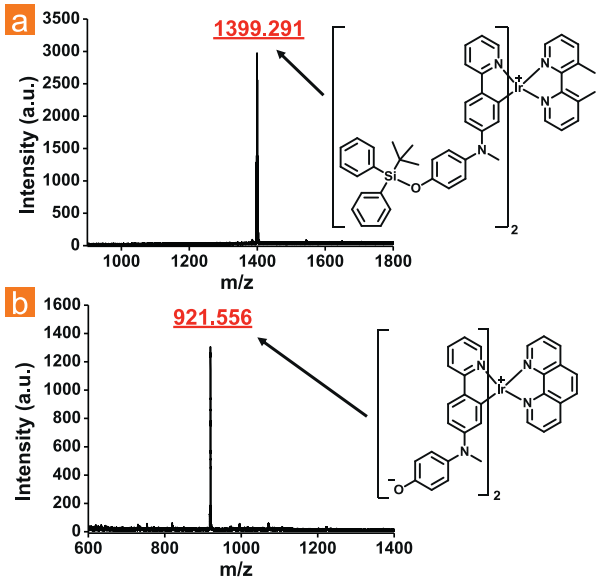

Fig. 4. MALDI-TOF-MS spectra of **Ir-AF** (a) and the MALDI-TOF-MS spectra of **Ir-AF** incubated with excessive fluoride anion (b) for 5 min.

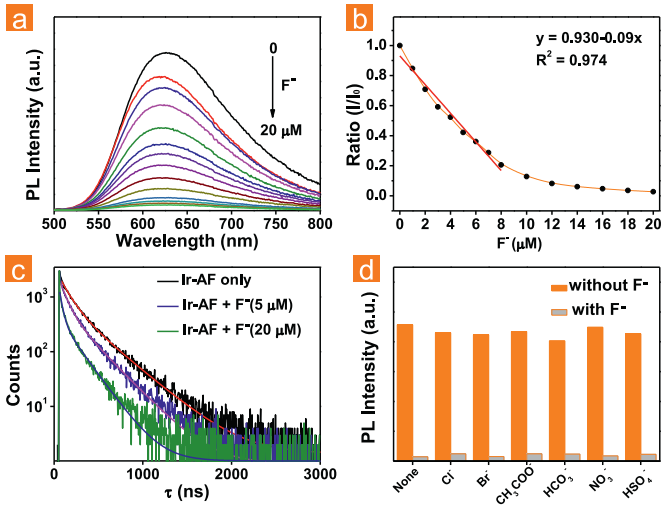

Fig. 5. Response of **Ir-AF** to fluoride anion. (a) Phosphorescence response of **Ir-AF** (10 μM) to different amounts of fluoride anion (0-20 μM) in aqueous solution. (b) The plot of phosphorescence intensity ratio (I/I_0) against the fluoride anion concentration. (c) Phosphorescence decays of **Ir-AF** in different amounts of fluoride anion, monitored at 622 nm. (d) Emission intensity of **Ir-AF** (10 μM) in aqueous solution containing other anions in the absence or presence of fluoride anion within 200 s. Excitation wavelength was 405 nm.

is qualified for detecting trace amounts of fluoride anion in the living cells.

To further justify the selectivity of **Ir-AF** to fluoride anion, several anions were selected as interference. As shown in the Fig. 5d, these anions hardly affected the phosphorescence intensity of **Ir-AF**, and the intensity changed remarkably only in presence of fluoride anion. These phenomenon are attributed to the good stability of **Ir-AF** and unique silicon-fluoride anion interactions. Additionally, the time-dependent intensity record illustrated that the phosphorescence intensity at 622 nm reached a plateau within 120 s after treatment with 20 μM fluoride anion, meaning that the progress of **Ir-AF** reacting with fluoride anion proceeded fast in aqueous solution (Fig. S3).

3.6. Fluoride anion imaging in living cells

The biocompatibility of **Ir-AF** for Hela cells, A549 cells and HepG2 cells was estimated by the 3-(4,5-dimethyl-2-thiazolyl)-2,5-diphenyltetrazolium bromide (MTT) assay, respectively (Fig. S4). When these cells were incubated with **Ir-AF** of 20 μM (a concentration higher than that used in cell imaging) for 24 h, the cell viabilities of three kinds of cells all kept above 70%, demonstrating that **Ir-AF** hardly has cytotoxicity, which can ensure its further applications in living cells.

Subsequently, the cell imaging experiments were conducted by confocal laser scanning microscopy. The luminescence signals from 550–650 nm were collected. As shown in Fig. S5a, the obvious luminescence could be observed from three kinds of cells, which indicated **Ir-AF** could enter into the living cells nonspecifically and formed the aggregates in living cells. Interestingly, the emission peak recorded by Lambda scanning model shifted from 625 to 560 nm. This may be because the polarity of intracellular environment is different from of that of aqueous solution that pulled down the levels of the ^{3}MLCT of **Ir-AF** (Fig. S5b). Furthermore, after illumination of build-in 405 nm laser source with the power of 100 μW for 60 s, the phosphorescence intensity from cells remains almost no change, stating that **Ir-AF** is a photo-stable imaging reagents (Fig. S6). Besides, the cells co-stained with **Ir-AF** and commercial nuclear dye Hoechst 33342 have been also investigated by time-resolved photoluminescence imaging. As shown in Fig. S7, upon excitation at 405 nm, the luminescence collected from 430–470 nm was located in the cell nucleus and the average photoluminescence lifetime was about 5 ns, while the luminescence collected from 550–650 nm distributed in the cell cytoplasm and the average photoluminescence lifetime reached around 150 ns. When 50 ns,

100 ns or 150 ns delay was exerted, only luminescence signals from the cell cytoplasm could be collected. These results illustrated that **Ir-AF** mainly gathered in cell cytoplasm and the long-lived phosphorescence of **Ir-AF** can be easily distinguished from the short-lived fluorescence of commercial fluorescent dye or background fluorescence via TRPI.

Based on the good comprehensive performance of **Ir-AF**, the fluoride anion imaging and sensing in live cells were conducted. After pretreated with **Ir-AF** (5 μM), Hela cells were subsequently incubated with PBS or different concentrations of fluoride anion for 30 min. The CLSM and TRPI images under different conditions were shown in Fig. 6 and S8. In the control group of PBS, the luminescence intensity collected from 550–650 nm was intensive and the average lifetime was about 150 ns. As the used fluoride anion increased from 0 to 20 μM, the recorded average phosphorescence intensity reduced from 2675 to 389 counts, and the average lifetime shortened from 149 to 75 ns. Accordingly, the signal intensity decreased markedly in the TGPI images which is recorded after a few dozens of nanoseconds delay. Meanwhile, similar quantitative analysis of phosphorescence intensity variation by flow cytometry was also obtained (Fig. S9). These results demonstrated that **Ir-AF** could function as a reliable probe for detecting intracellular fluoride anion.

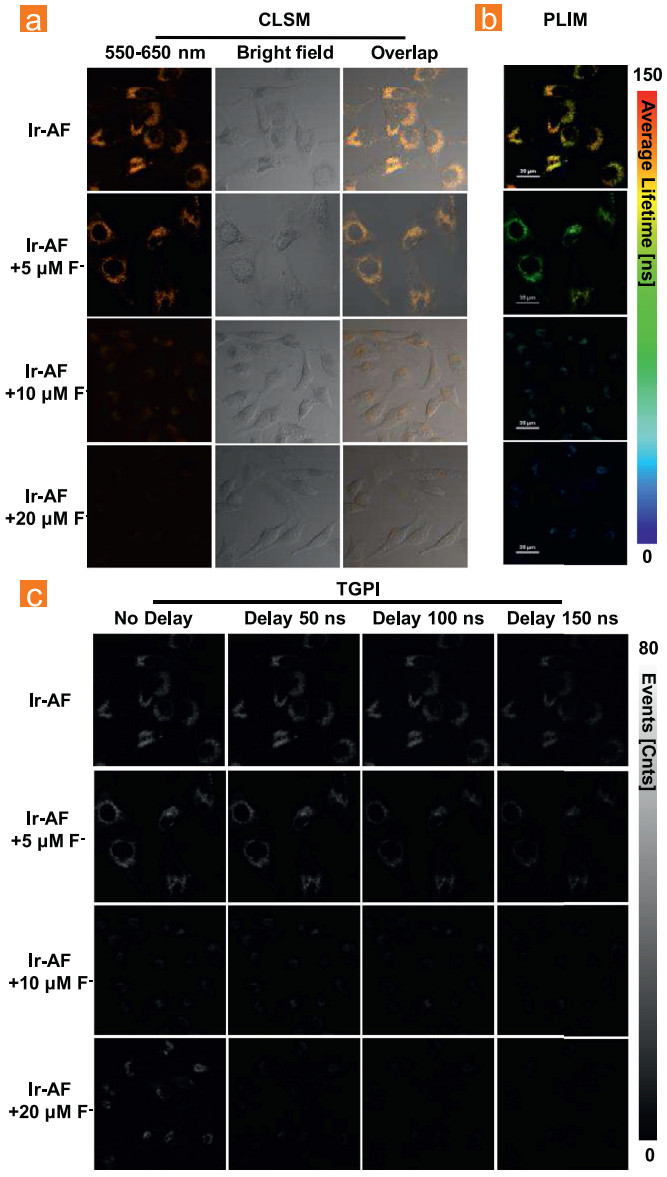

Fig. 6. Confocal laser scanning images (CLSM) (a), photoluminescence lifetime images (PLIM) (b) and time-gated photoluminescence images (TGPI) (c) of living Hela cells labeled with **Ir-AF** were subsequently treated with PBS, different amounts of fluoride anion (5 μM, 10 μM and 20 μM), respectively. The orange channels in CLSM images were acquired by collecting the photoluminescence from 550 to 650 nm and photoluminescence was collected through longpass filter ($\geq$ 550 nm) for PLIM and TGPI images. Excitation wavelength was 405 nm.

4. Conclusion

In conclusion, a novel cationic iridium(III) complex fluoride anion probe **Ir-AF** which exhibits aggregation-induced phosphorescent emission was designed and synthesized. Distinctively, its working mechanism is based on the synergistic effect including enhancement of PET process and attenuation of AIPE effect. Owing to its fine photostability, high sensitivity, excellent selectivity, good biocompatibility, and long emission lifetime, **Ir-AF** has been used for fluoride anion imaging and sensing in living cells with high signal to noise ratio via time-resolved photoluminescence imaging. Next, work will focus on regulating its water-dispersibility and developing near-infrared-excited probes with aggregation-induced phosphorescent emission for fluoride anion imaging in vivo.

Declaration of Competing Interest

The authors declare that they have no known competing financial interests or personal relationships that could have appeared to influence the work reported in this paper.

Acknowledgments

This work was supported by the National Natural Science Foundation of China (21501098 and 21671108), Science and Technology Research Project of Jiangxi Provincial Department of

Education (GJJ190350), Natural Science Foundation of Jiangxi Province (20202BAB214012) and the open research fund of Key Laboratory for Organic Electronics and Information Displays.

Supplementary materials

Supplementary material associated with this article can be found, in the online version, at doi:10.1016/j.jorganchem.2020.121644.

Appendix A. Supplementary data

Supplementary data (details of the synthesis, NMR, cell culture, imaging) to this article can be found online at https://doi.org/10.1016/j.jorganchem.

References

[1] S. Jagtap, M.K. Yenkie, N. Labhsetwar, S. Rayalu, Fluoride in drinking water and defluoridation of water, Chem. Rev. 112 (2012) 2454–2466.
[2] M. Kleerekoper, The role fluoride in the prevention of osteoporosis, Endocrinol. Metab. Clin. North. Am. 27 (1998) 441–452.
[3] R.G. Foulkes, The precautionary principle and "evidence-based dentistry", Fluoride 40 (2007) 4–6.
[4] P. Connet, Professionals mobilize to end water fluoridation worldwide, Fluoride 40 (2007) 155–158.
[5] R.J. Carton, Review of the 2006 United States National Research Council report: Fluoride in drinking water, Fluoride 39 (2006) 163–172.
[6] H.S. Horowitz, The 2001 CDC recommendations for using fluoride to prevent and control dental caries in the United States, J. Public Health Dent. 63 (2003) 3–8.
[7] E.T. Everett, Fluoride's effects on the formation of teeth and bones, and the influence of genetics, J. Dent. Res. 90 (2011) 552–560.
[8] Y. Shivarajashankara, A. Shivashankara, Neurotoxic effects of fluoride in endemic skeletal fluorosis and in experimental chronic fluoride toxicity, J. Clin. Diagn. Res. (2012) 740–744.
[9] Y.P. Reddy, S.K. Tiwari, A.P. Shaik, A. Alsaeed, A. Sultana, P.K. Reddy, Effect of sodium fluoride on neuroimmunological parameters, oxidative stress and antioxidative defenses, Toxicol. Mech. Methods. 24 (2014) 31–36.
[10] A.L. Choi, G. Sun, Y. Zhang, P. Grandjean, Developmental fluoride neurotoxicity: A systematic review and meta-analysis, Environ. Health Perspect. 120 (2012) 1362–1368.
[11] B. Spittle, Neurotoxic effects of fluoride, Fluoride 44 (2011) 117–124.
[12] H. Yahyavi, M. Kaykhaii, M. Mirmoghaddam, Recent developments in methods of analysis for fluoride determination, Critical Rev. Anal. Chem. 46 (2016) 106–121.
[13] A. Dhillon, M. Nair, D. Kumar, Analytical methods for determination and sensing of fluoride in biotic and abiotic sources: A review, Anal. Methods 8 (2016) 5338–5352.
[14] H. Yiping, W. Caiyun, Ion chromatography for rapid and sensitive determination of fluoride in milk after headspace single-drop microextraction with in situ generation of volatile hydrogen fluoride, Anal. Chim. Acta. 661 (2010) 161–166.
[15] R. De Marco, G. Clarke, B. Pejcic, Ion-selective electrode potentiometry in environmental analysis, Electroanalysis 19 (2007) 1987–2001.
[16] J.K. Willmann, N. van Bruggen, L.M. Dinkelborg, S.S. Gambhir, Molecular imaging in drug development, Nat. Rev. Drug Discov. 7 (2008) 591–607.
[17] R. Weissleder, M.J. Pittet, Imaging in the era of molecular oncology, Nature 452 (2008) 580–589.
[18] X. Huang, J. Song, B.C. Yung, X. Huang, Y. Xiong, X. Chen, Ratiometric optical nanoprobes enable accurate molecular detection and imaging, Chem. Soc. Rev. 47 (2018) 2873–2920.
[19] X. Li, R. Tao, L. Hong, J. Cheng, Q. Jiang, Y. Lu, M. Liao, W. Ye, N. Lu, F. Han, Y. Hu, Visualizing peroxynitrite fluxes in endothelial cells reveals the dynamic progression of brain vascular injury, J. Am. Chem. Soc. 137 (2015) 12296–12303.
[20] J. Huang, J. Li, Y. Lyu, Q. Miao, K. Pu, Molecular optical imaging probes for early diagnosis of drug-induced acute kidney injury, Nat. Mater. 18 (2019) 1133–1143.
[21] Q. Zhao, F. Li, C. Huang, Phosphorescent chemosensors based on heavy-metal complexes, Chem. Soc. Rev. 39 (2010) 3007–3030.
[22] D.L. Ma, C. Wu, H. Liu, K.J. Wu, C.H. Leung, Luminescence approaches for the rapid detection of disease-related receptor proteins using transition metal-based probes, J. Mater. Chem. B 8 (2020) 3249–3260.
[23] K.Y. Zhang, Q. Yu, H. Wei, S. Liu, Q. Zhao, W. Huang, Long-lived emissive probes for time-resolved photoluminescence bioimaging and biosensing, Chem. Rev. 118 (2018) 1770–1839.
[24] D.L. Ma, M. Wang, C. Liu, X. Miao, T.S. Kang, C.H. Leung, Metal complexes for the detection of disease-related protein biomarkers, Coord. Chem. Rev. 324 (2016) 90–105.
[25] L. Hao, Z.W. Li, D.Y. Zhang, L. He, W. Liu, J. Yang, C.P. Tan, L.N. Ji, Z.W. Mao, Monitoring mitochondrial viscosity with anticancer phosphorescent Ir(III) complexes via two-photon lifetime imaging, Chem. Sci. 10 (2019) 1285–1293.
[26] L. He, C.P. Tan, R.R. Ye, Y.Z. Zhao, Y.H. Liu, Q. Zhao, L.N. Ji, Z.W. Mao, Theranostic iridium(III) complexes as one- and two-photon phosphorescent trackers to monitor autophagic lysosomes, Angew. Chem. Int. Ed. 53 (2014) 12137–12141.
[27] P.Y. Ho, C.L. Ho, W.Y. Wong, Recent advances of iridium(III) metallophosphors for health-related applications, Coord. Chem. Rev. 413 (2020) 213267.
[28] Q. Zhao, C. Zhang, S. Liu, Y. Liu, K.Y. Zhang, X. Zhou, J. Jiang, W. Xu, T. Yang, W. Huang, Dual-emissive polymer dots for rapid detection of fluoride in pure water and biological systems with improved reliability and accuracy, Sci. Rep. 5 (2015) 16420.
[29] S. Liu, J. Zhang, D. Shen, H. Liang, X. Liu, Q. Zhao, W. Huang, Reaction-based phosphorescent nanosensor for ratiometric and time-resolved luminescence imaging of fluoride in live cells, Chem. Commun. 51 (2015) 12839–12842.
[30] Z. Chen, P. Yan, L. Zou, M. Zhao, J. Jiang, S. Liu, K.Y. Zhang, W. Huang, Q. Zhao, Using ultrafast responsive phosphorescent nanoprobe to visualize elevated peroxynitrite in vitro and in vivo via ratiometric and time-resolved photoluminescence imaging, Adv. Healthcare Mater. (7) (2018) 1800309.
[31] Z. Chen, X. Meng, M. Xie, Y. Shi, L. Zou, S. Guo, J. Jiang, S. Liu, Q. Zhao, A self-calibrating phosphorescent polymeric probe for measuring pH fluctuations in subcellular organelles and the zebrafish digestive tract, J. Mater. Chem. C 8 (2020) 2265–2271.
[32] H. Zhang, Z. Zhao, A.T. Turley, L. Wang, P.R. McGonigal, Y. Tu, Y. Li, Z. Wang, R.T.K. Kwok, J.W.Y. Lam, B.Z. Tang, Aggregate science: from structures to properties, Adv. Mater. 32 (2020) 2001457.
[33] B. Manimaran, P. Thanasekaran, T. Rajendran, R.J. Lin, I.J. Chang, G.H. Lee, S.M. Peng, S. Rajagopal, K.L. Lu, Luminescence enhancement induced by aggregation of alkoxy-bridged rhenium(I) molecular rectangles, Inorg. Chem. 41 (2002) 5323–5325.
[34] Q. Zhao, L. Li, F. Li, M. Yu, Z. Liu, T. Yi, C. Huang, Aggregation-induced phosphorescent emission (AIPE) of iridium(III) complexes, Chem. Commun. (2008) 685–687.
[35] L. Wang, Z. Gao, C. Liu, X. Jin, A diphenylamino-substituted cationic cyclometalated Ir(III) complex: its aggregationinduced phosphorescent emission and oxygen sensing properties, Mater. Chem. Front. 3 (2019) 1593–1600.
[36] Y. Jiang, G. Li, D. Zhu, Z. Su, M.R. Bryce, An AIE-active phosphorescent Ir(III) complex with piezochromic luminescence (PCL) and its application for monitoring volatile organic compounds (VOCs), J. Mater. Chem. C 5 (2017) 12189–12193.
[37] W. Che, G. Li, X. Liu, K. Shao, D. Zhu, Z. Su, M.R. Bryce, Selective sensing of 2,4,6-trinitrophenol (TNP) in aqueous media with "aggregation-induced emission enhancement" (AIEE)-active iridium(III) complexes, Chem. Commun. 54 (2018) 1730–1733.
[38] C. Climenta, P. Alamb, S.S. Pashab, G. Kaurc, A.R. Choudhuryc, I.R. Laskarb, P. Alemanya, D. Casanova, Dual emission and multi-stimuli-response in iridium(III) complexes with aggregation-induced enhanced emission: Application to quantitative CO2 detection, J. Mater. Chem. C 5 (2017) 7784–7798.
[39] K. Ohno, T. Sakata, M. Shiiba, A. Nagasawa, T. Fujihara, A water-soluble cyclometalated iridium(III) complex for pH sensing based on aggregationinduced enhanced phosphorescence, Dalton Trans 48 (2019) 8068–8075.
[40] D. Li, G. Li, W. Che, D. Zhu, Z. Su, A remarkable phosphorescent sensor for acid-base vapours based on an AIPE-active Ir(III) complex, Dalton Trans. 48 (2019) 1955–1959.
[41] J. Ma, Y. Zeng, Y. Liu, D. Wu, Thermostable polymeric nanomicelles of iridium (III) complexes with aggregation-induced phosphorescence emission characteristics and their recyclable double-strand DNA monitoring, J. Mater. Chem. B 5 (2017) 123–133.
[42] J. Wu, Y. Li, C. Tan, X. Wang, Y. Zhang, J. Song, J. Qu, W.Y. Wong, Aggregation-induced near-infrared emitting platinum(II) terpyridyl complex: cellular characterisation and lysosome-specific localization, Chem. Commun. 54 (2018) 11144–11147.
[43] X. Yang, L. Yue, Y. Yu, B. Liu, J. Dang, Y. Sun, G. Zhou, Z. Wu, W.Y. Wong, Strategically formulating aggregation-induced emission-active phosphorescent emitters by restricting the coordination skeletal deformation of Pt(II) complexes containing two independent monodentate ligands, Adv. Optical Mater. 8 (2020) 2000079.
[44] Z. Chen, X. Meng, L. Zou, M. Zhao, S. Liu, P. Tao, J. Jiang, Q. Zhao, A dual-emissive phosphorescent polymeric probe for exploring drug-induced liver injury via imaging of peroxynitrite elevation in vivo, ACS Appl. Mater. Interfaces 12 (2020) 12383–12394.
[45] P. Ruiz-Castillo, S.L. Buchwald, Applications of palladium-catalyzed C-N cross–coupling reactions, Chem. Rev. 116 (2016) 12564–12649.
[46] M. Nonoyama, Benzo[h]quinolin-10-yl-N Iridium(III) complexes, Bull. Chem. Soc. Jpn. 47 (1974) 767–768.
[47] P. Tao, Y. Miao, H. Wang, B. Xu, Q. Zhao, High-performance organic electroluminescence: Design from organic light-emitting materials to devices, Chem. Rec. 19 (2019) 1531–1561.